# Supplementary information: Long-term $NO_X$ measurements in the remote marine tropical troposphere

Simone T. Andersen[1*], Lucy J. Carpenter[1], Beth S. Nelson[1], Luis Neves[1], Katie A. Read[1,2], Chris Reed[3], Martyn Ward[1], Matthew J. Rowlinson[1,2], James D. Lee[1,2]

[1]Wolfson Atmospheric Chemistry Laboratories (WACL), Department of Chemistry, University of York, Heslington, York, YO10 5DD, UK.

[2]National Centre for Atmospheric Science (NCAS), University of York, Heslington, York, YO10 5DD, UK.

[3]FAAM Airborne Laboratory, Building 146, Cranfield University, Cranfield, MK43 0AL, UK.

[*]Corresponding author: sta516@york.ac.uk

# 1. $O_3$ Correction:

NO and $NO_2$ are in photo-stationary state in the atmosphere, where NO reacts with $O_3$ to give $NO_2$ and $NO_2$ is photolysed to NO:

$$NO + O_3 \rightarrow NO_2 + O_2 \qquad k_{NO+O3} \qquad \text{(S1)}$$

$$NO_2 + h\nu \rightarrow NO + O \qquad J_C \qquad \text{(S2)}$$

When measuring NO and $NO_2$, NO continues to react with ambient $O_3$ in the sample line to the instrument, however, no photolysis occurs in the sample line causing an underestimation of NO and an overestimation of $NO_2$. This can be corrected using the equations described below.

## 1.1 NO correction

Since NO only reacts with $O_3$ in the line and is not photolysed back to NO as it would be in the atmosphere during daylight, the decrease in NO can be described by a simple rate equation:

$$\frac{d[NO]}{dt} = -k_{NO+O3}[O_3][NO] = -k_{O3}[NO] \qquad \text{(SI)}$$

where $k_{NO+O3}[O_3] = k_{O3}$. By integrating between time = 0 and the time it takes to reach the reaction cell ($t = t_{E1}$) the following is obtained:

$$\ln\left(\frac{[NO]_{E1}}{[NO]_0}\right) = -k_{O3} \times t_{E1} \qquad \text{(SII)}$$

$$[NO]_0 = [NO]_{E1} \times e^{k_{O3} \times t_{E1}} \qquad \text{(SIII)}$$

where $[NO]_0$ and $[NO]_{E1}$ are the NO mixing ratio at the inlet and that measured by the PMT, respectively.

## 1.2 $NO_2$ correction

$NO_2$ is measured by converting it photolytically into NO and reacting the NO with $O_3$ to produce excited state $NO_2$ which emits chemiluminescent light as it drops to the ground state.

The measured mixing ratio of $NO_2$ is calculated from the NO signals with ($[NO]_{E2}$) and without ($[NO]_{E1}$) the converter on and the conversion efficiency of the converter ($S_C$):

$$[NO_2]_M = \frac{[NO]_{E2} - [NO]_{E1}}{S_c} \quad \text{(SIV)}$$

To correct the measured $NO_2$ mixing ratio for reactions with $O_3$, the following needs to be taken into account:

- NO reacts with $O_3$ in the line before reaching the converter
- $NO_2$ is photolysed into NO at the same time as NO continues to react with $O_3$ inside the converter

The photo-stationary state of NO and $NO_2$ inside the converter can be described by the following equations:

$$[NO]_{PSS} = [NO]_0 + \Delta NO \quad \text{(SV)}$$

$$[NO_2]_{PSS} = [NO_2]_0 - \Delta NO_2 \quad \text{(SVI)}$$

Where $[NO]_{PSS}$ and $[NO_2]_{PSS}$ are the photo-stationary state mixing ratios of NO and $NO_2$, respectively, $[NO]_0$ and $[NO_2]_0$ are the mixing ratios of NO and $NO_2$ at the entrance of the inlet, and $\Delta NO$ and $\Delta NO_2$ are the change in NO and $NO_2$ inside the converter. The change in NO and $NO_2$ will be equal since the only reactions occurring are reactions (S1) and (S2). Thus, the photo-stationary state can be written as:

$$[NO]_{PSS} = [NO]_0 + [NO_2]_0 - [NO_2]_{PSS} \quad \text{(SVII)}$$

$$[NO_2]_{PSS} = [NO_2]_0 - ([NO]_{PSS} - [NO]_0) = [NO_2]_0 + [NO]_0 - [NO]_{PSS} \quad \text{(SVIII)}$$

In photo-stationary state, reactions (S1) and (S2) react with the same rate, which can be written as:

$$k_{O3} \times [NO]_{PSS} = J_C \times [NO_2]_{PSS} \quad \text{(SIX)}$$

where $J_C$ is the photolysis rate of the converter. Combining equation (SVIII) and (SIX) gives the following equations for the photo-stationary state of NO:

$$[NO]_{PSS} = \frac{J_C}{k_{O3}} \times [NO_2]_{PSS} = \frac{J_C}{k_{O3}} \times ([NO_2]_0 + [NO]_0 - [NO]_{PSS}) \quad \text{(SX)}$$

$$[NO]_{PSS} = \frac{J_C}{k_{O3}} \times ([NO_2]_0 + [NO]_0) - \frac{J_C}{k_{O3}} \times [NO]_{PSS} \quad \text{(SXI)}$$

$$\left(1+\frac{\mathrm{J_C}}{k_{\mathrm{O_3}}}\right)\times[\mathrm{NO}]_{\mathrm{PSS}}=\left(\frac{k_{\mathrm{O_3}}+\mathrm{J_C}}{k_{\mathrm{O_3}}}\right)\times[\mathrm{NO}]_{\mathrm{PSS}}=\frac{\mathrm{J_C}}{k_{\mathrm{O_3}}}\times([\mathrm{NO_2}]_0+[\mathrm{NO}]_0) \quad \text{(SXII)}$$

$$[\mathrm{NO}]_{\mathrm{PSS}}=\left(\frac{k_{\mathrm{O_3}}}{k_{\mathrm{O_3}}+\mathrm{J_C}}\right)\times\frac{\mathrm{J_C}}{k_{\mathrm{O_3}}}\times([\mathrm{NO_2}]_0+[\mathrm{NO}]_0)=\left(\frac{\mathrm{J_C}}{k_{\mathrm{O_3}}+\mathrm{J_C}}\right)\times([\mathrm{NO_2}]_0+[\mathrm{NO}]_0) \quad \text{(SXIII)}$$

By combining equations (SIX) and (SXIII), the photo-stationary state of $NO_2$ in the converter can be obtained:

$$[\mathrm{NO_2}]_{\mathrm{PSS}}=\frac{k_{\mathrm{O_3}}}{\mathrm{J_C}}[\mathrm{NO}]_{\mathrm{PSS}}=\frac{k_{\mathrm{O_3}}}{\mathrm{J_C}}\times\left(\frac{\mathrm{J_C}}{k_{\mathrm{O_3}}+\mathrm{J_C}}\right)\times([\mathrm{NO_2}]_0+[\mathrm{NO}]_0) \quad \text{(SXIV)}$$

$$[\mathrm{NO_2}]_{\mathrm{PSS}}=\left(\frac{k_{\mathrm{O_3}}}{k_{\mathrm{O_3}}+\mathrm{J_C}}\right)\times([\mathrm{NO_2}]_0+[\mathrm{NO}]_0) \quad \text{(SXV)}$$

The photolysis rate inside the converter is given by:

$$\mathrm{J_C}=\frac{-\ln(1-\mathrm{S_C})}{\mathrm{t_{C2}}} \quad \text{(SXVI)}$$

where $t_{C2}$ is the time the air is in the converter while it is on.

Inside the converter, the NO mixing ratio moves towards photo-stationary state ($[NO]_{PSS}$) with a rate of $k_{O3}+ J_C$ since some of the $NO_2$ being photolysed to NO in the converter will react with $O_3$ in the sample to regenerate $NO_2$. This can be described by equation (SXVII), where $[NO]_L$ is the NO mixing ratio at the entrance of the converter:

$$[\mathrm{NO}]_{\mathrm{E2}}=[\mathrm{NO}]_{\mathrm{PSS}}-([\mathrm{NO}]_{\mathrm{PSS}}-[\mathrm{NO}]_{\mathrm{L}})\times\mathrm{e}^{\{-(k_{\mathrm{O_3}}+\mathrm{J_C})\times\mathrm{t_{C2}}\}} \quad \text{(SXVII)}$$

$$[\mathrm{NO}]_{\mathrm{E2}}=[\mathrm{NO}]_{\mathrm{PSS}}-[\mathrm{NO}]_{\mathrm{PSS}}\times\mathrm{e}^{\{-(k_{\mathrm{O_3}}+\mathrm{J_C})\times\mathrm{t_{C2}}\}}+[\mathrm{NO}]_{\mathrm{L}}\times\mathrm{e}^{\{-(k_{\mathrm{O_3}}+\mathrm{J_C})\times\mathrm{t_{C2}}\}} \quad \text{(SXVIII)}$$

$$[\mathrm{NO}]_{\mathrm{E2}}=[\mathrm{NO}]_{\mathrm{PSS}}\times\left(1-\mathrm{e}^{\{-(k_{\mathrm{O_3}}+\mathrm{J_C})\times\mathrm{t_{C2}}\}}\right)+[\mathrm{NO}]_{\mathrm{L}}\times\mathrm{e}^{\{-(k_{\mathrm{O_3}}+\mathrm{J_C})\times\mathrm{t_{C2}}\}} \quad \text{(SXIX)}$$

The NO mixing ratio at the entrance of the converter can be estimated from the loss of NO to $O_3$ in the line in the same way as the ozone corrected NO mixing ratio could be determined:

$$[\mathrm{NO}]_{\mathrm{L}}=[\mathrm{NO}]_0\times\mathrm{e}^{(-k_{\mathrm{O_3}}\times\mathrm{t_L})}=[\mathrm{NO}]_{\mathrm{E1}}\times\mathrm{e}^{(k_{\mathrm{O_3}}\times\mathrm{t_{E1}})}\times\mathrm{e}^{(-k_{\mathrm{O_3}}\times\mathrm{t_L})} \quad \text{(SXX)}$$

$$[\mathrm{NO}]_{\mathrm{L}}=[\mathrm{NO}]_{\mathrm{E1}}\times\mathrm{e}^{(k_{\mathrm{O_3}}\times\mathrm{t_{C1}})} \quad \text{(SXXI)}$$

Equations (SXIX) and (SXXI) are combined to give equation (SXXII):

$$[\mathrm{NO}]_{\mathrm{E2}}=[\mathrm{NO}]_{\mathrm{PSS}}\times\left(1-\mathrm{e}^{\{-(k_{\mathrm{O_3}}+\mathrm{J_C})\times\mathrm{t_{C2}}\}}\right)+[\mathrm{NO}]_{\mathrm{E1}}\times\mathrm{e}^{\{-(k_{\mathrm{O_3}}+\mathrm{J_C})\times\mathrm{t_{C2}}+k_{\mathrm{O_3}}\times\mathrm{t_{C1}}\}} \quad \text{(SXXII)}$$

$[NO]_{PSS}$ is isolated to give equation (SXXIII):

$$[NO]_{PSS} = \frac{[NO]_{E2} - [NO]_{E1} \times e^{\{-(k_{O3}+J_C)\times t_{C2} + k_{O3}\times t_{C1}\}}}{1 - e^{\{-(k_{O3}+J_C)\times t_{C2}\}}} \quad \text{(SXXIII)}$$

Lastly equations (SXIII) and (SXXIII) are combined to give equation (SXXIV) and rearranged to give the ozone corrected mixing ratio in equation (SXXV):

$$\frac{J_C}{J_C + k_{O3}} \times ([NO]_0 + [NO_2]_0) = \frac{[NO]_{E2} - [NO]_{E1} \times e^{\{-(k_{O3}+J_C)\times t_{C2} + k_{O3}\times t_{C1}\}}}{1 - e^{\{-(k_{O3}+J_C)\times t_{C2}\}}} \quad \text{(SXXIV)}$$

$$[NO_2]_0 = \left(\frac{J_C + k_{O3}}{J_C}\right) \times \left(\frac{[NO]_{E2} - [NO]_{E1} \times e^{\{-(k_{O3}+J_C)\times t_{C2} + k_{O3}\times t_{C1}\}}}{1 - e^{\{-(k_{O3}+J_C)\times t_{C2}\}}}\right) - [NO]_0 \quad \text{(SXXV)}$$

## 1.3 Low $O_3$ concentration

At low $O_3$ concentrations $k_{O3}$ tends towards 0 and becomes very small compared to $J_C$, such that the calculations for NO and $NO_2$ become:

$$[NO]_0 = [NO]_{E1} \quad \text{(SXXVI)}$$

$$[NO_2]_0 = \left(\frac{J_C}{J_C}\right) \times \left(\frac{[NO]_{E2} - [NO]_{E1} \times e^{\{-J_C \times t_{C2}\}}}{1 - e^{\{-J_C \times t_{C2}\}}}\right) - [NO]_{E1} \quad \text{(SXXVII)}$$

$$[NO_2]_0 = \frac{[NO]_{E2} - [NO]_{E1} \times e^{\{-J_C \times t_{C2}\}} - [NO]_{E1} + [NO]_{E1} \times e^{\{-J_C \times t_{C2}\}}}{1 - e^{\{-J_C \times t_{C2}\}}} \quad \text{(SXXVIII)}$$

$$[NO_2]_0 = \frac{[NO]_{E2} - [NO]_{E1}}{1 - e^{\{-J_C \times t_{C2}\}}} = \frac{[NO]_{E2} - [NO]_{E1}}{1 - e^{\left\{-\left(\frac{-\ln(1-S_C)}{t_{C2}}\right)\times t_{C2}\right\}}} = \frac{[NO]_{E2} - [NO]_{E1}}{S_C} \quad \text{(SXXIX)}$$

## 1.4 Example calculation

An example calculation of the $O_3$ corrections is shown below, assuming a conversion efficiency of 50% ($S_C$ = 50%), a time of 3.3s from the inlet to the converter ($t_L$ = 3.3s), a residence time of 1s for the sample in the converter whether the converter is on or not ($t_{C1}$=$t_{C2}$=1s), an ozone mixing ratio of 30 ppbV, a temperature of at 298K and therefore, using k($O_3$ + NO) = 1.8 × $10^{-14}$ $cm^3$ $molecule^{-1}$ $s^{-1}$, a $k_{O3}$ = 0.013 $s^{-1}$.

We start with uncorrected mixing ratios (i.e. measured mixing ratios) of $[NO]_M$ = 10 pptV and $[NO_2]_M$ = 30 pptV:

$[NO]_{E1}$ = 10 pptV

112 $$[\mathrm{NO}]_{\mathrm{E2}} = 30\mathrm{pptV} \times 0.5 + 10\mathrm{pptV} = 25\mathrm{pptV}$$

113 $$\mathrm{J_C} = \frac{-\ln(1-\mathrm{S_C})}{\mathrm{t_{C2}}} = \frac{-\ln(1-0.5)}{1\mathrm{s}} = 0.69\ \mathrm{s}^{-1}$$

114 $$[\mathrm{NO}]_0 = [\mathrm{NO}]_{\mathrm{E1}} \times \mathrm{e}^{k_{\mathrm{O3}} \times \mathrm{t_{E1}}} = 10\ \mathrm{pptV} \times \mathrm{e}^{0.013\mathrm{s}^{-1} \times 4.3\mathrm{s}} = 10.6\ \mathrm{pptV}$$

115 $$[\mathrm{NO_2}]_0 = \left(\frac{\mathrm{J_C} + k_{\mathrm{O3}}}{\mathrm{J_C}}\right) \times \left(\frac{[\mathrm{NO}]_{\mathrm{E2}} - [\mathrm{NO}]_{\mathrm{E1}} \times \mathrm{e}^{\{-(k_{\mathrm{O3}} + \mathrm{J_C}) \times \mathrm{t_{C2}} + k_{\mathrm{O3}} \times \mathrm{t_{C1}}\}}}{1 - \mathrm{e}^{\{-(k_{\mathrm{O3}} + \mathrm{J_C}) \times \mathrm{t_{C2}}\}}}\right) - [\mathrm{NO}]_0$$

116 $$= \left(\frac{0.69\mathrm{s}^{-1} + 0.013)}{0.69\mathrm{s}^{-1}}\right)$$

117 $$\times \left(\frac{25\mathrm{pptV} - 10\mathrm{pptV} \times \mathrm{e}^{\{-(0.013\mathrm{s}^{-1} + 0.69\mathrm{s}^{-1}) \times 1\mathrm{s} + 0.013\mathrm{s}^{-1} \times 1\mathrm{s}\}}}{1 - \mathrm{e}^{\{-(0.013\mathrm{s}^{-1} + 0.69\mathrm{s}^{-1}) \times 1\mathrm{s}\}}}\right) - 10.6\ \mathrm{pptV}$$

118 $$= 1.02 \times 39.6 - 10.6 = 29.7\ \mathrm{pptV}$$

119 This gives a small increase in NO mixing ratio (0.6 pptV or 5.7%) and a small decrease
120 (0.3 pptV or 1%) in $NO_2$ mixing ratio under these conditions.

121

# 2. Uncertainty Analysis:

The uncertainty of a measurement is given as an interval at a confidence level, which describes how certain it is that the true value is within the interval. The interval can be determined from the spread of data, which can be described by several probability distributions. The most common are normal and rectangular distributions. A normal distribution is used when most of the measurements are centred around the mean. The signal-to-noise is reduced by approximately $1/\sqrt{(\text{number of averaging points})}$ when averaging the measurements. The uncertainty in the mean of the measurements are estimated using equation (SXXX). To get an uncertainty at the 95 percent confidence interval 2 standard deviations (σ) are used. A rectangular distribution is when the probability of each measurement is equal. The 1σ uncertainty is estimated from the half-width of the distribution and the 2σ uncertainty is estimated from the full width of the distribution as shown in equation (SXXXI). The hourly precision and uncertainty of the instrument are estimated to characterize the uncertainties at the 95 percent confidence interval (Bell, 1999).

$$\text{Normal distribution uncertainty (u)} = \frac{2\sigma}{\sqrt{\text{number of averaging point}}} \qquad \text{(SXXX)}$$

$$\text{Rectangular distribution uncertainty} = \frac{\text{full}-\text{width}}{\sqrt{3}} \qquad \text{(SXXXI)}$$

The hourly precision is estimated from the zero count variability, which is directly related to the photon-counting precision of the PMT. The hourly mean ($\bar{x}$) of the zero measurements is subtracted from each individual measurement of the respective hour ($x - \bar{x}$) to give hourly frequency distributions. Photon-counting frequency distributions are best described by a Poisson distribution, however, at high photon-counting rates become indistinguishable from a Gaussian distribution (Silvia and Skilling, 2006). With a yearly mean background count rate of ~1400-3000 count $s^{-1}$ between 2014 and 2019, the frequency distributions can be assumed as Gaussian. Examples of hourly frequency distributions can be observed in figure S1. The standard deviation of each hourly frequency distribution is calculated and divided by the interpolated sensitivity to give a 2σ NO precision for 1 s data of 23.4 ± 20.3 pptV for the hours between January 2014 and August 2019. The 2σ NO precision for hourly averaged data is 0.96 ± 0.89 pptV. The hourly precisions reported here are in good agreement with the previously reported 1σ precision of 0.30 pptV (Reed et al., 2017) and the 2σ precision of 0.6-1.7 pptV (Lee et al., 2009). The $NO_2$ precisions are determined by taking the conversion efficiency of

the respective converters into account. The hourly 2σ $NO_2$ precision for hourly averaged data between March 2017 and August 2019 becomes 1.45 ± 0.82 pptV and 2.74 ± 2.18 pptV for the BLC and PLC, respectively. The determined $NO_2$ precisions are within the interval of previously reported precisions for the same instrument (Lee et al., 2009; Reed et al., 2017).

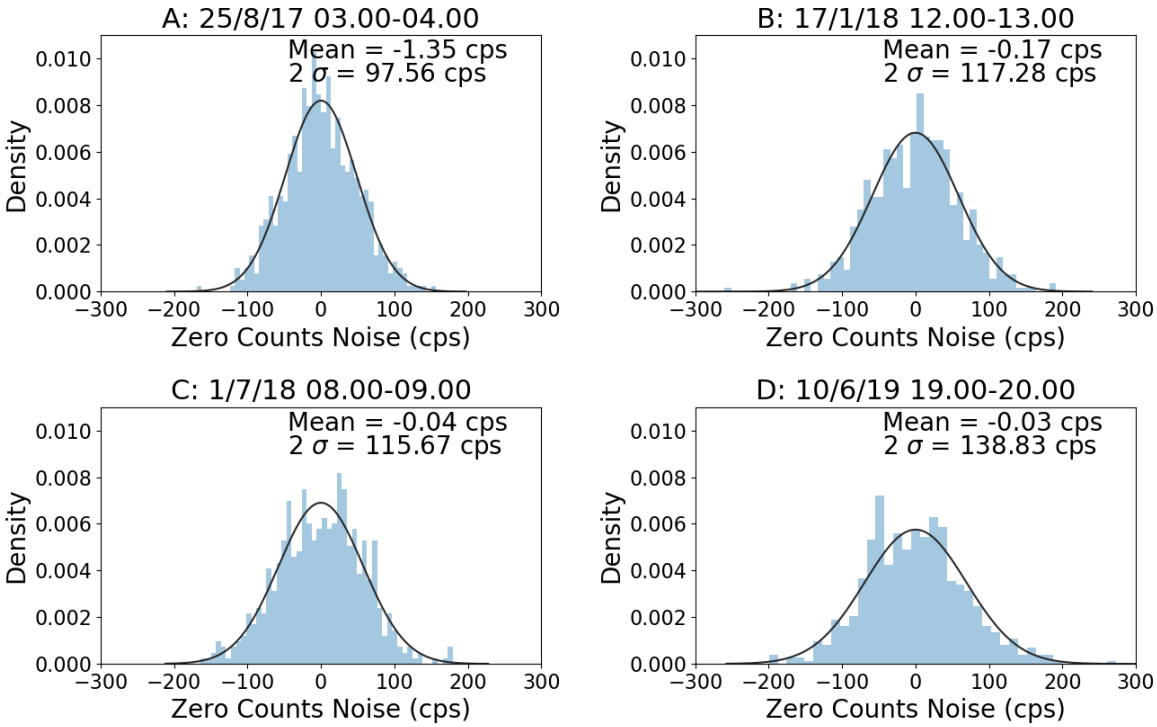


Figure S1: Examples of hourly frequency distributions of the calculated zero variability.

The uncertainty of the hourly measurements is estimated by combining all the uncertainties associated with the measurements. This includes uncertainties in the calibrations, artefact determinations, and $O_3$ corrections as well as the precision of the instrument. The precision of the NO and $NO_2$ measurements are both included in the total uncertainty of the $NO_2$ measurements as the NO measurements are subtracted from the $NO_2$ measurements. Each term is converted into pptV to be able to combine them. All the uncertainties are combined using uncertainty propagation:

$$\text{Accuarcy} = \sqrt{\text{Precision}^2 + \text{Artefact}^2 + \text{Calibration}^2 + \text{O}_3\ \text{Correction}^2} \qquad \text{(SXXXII)}$$

Uncertainty in the calibrations is caused by uncertainty in the flow of calibration gas, the concentration of the calibration gas, the sensitivity, and the conversion efficiency as well as the drift in the sensitivity and conversion efficiency between each calibration. The total uncertainty in the calibrations is determined as the propagation of each term. Each term is calculated as a percentage to be able to combine them before converting the total calibration uncertainty to

pptV to combine it with the other uncertainty terms. According to the manufacturers the sample and calibration mass flow controllers have an uncertainty of 1%, which has been confirmed by a gillibrator bubble flowmeter. The uncertainty of the concentration of the NO standard used for calibration is known to ±1% (British Oxygen Company (BOC), certified to UK National Physical Laboratory (NPL) standard) (BOC certifies that $NO/N_2$ standards are stable for 5 years). To estimate the uncertainty in the sensitivity and conversion efficiency, the uncertainties in each measurement used to determine them must be estimated. Equation IV and V describe the calculation of the sensitivity and conversion efficiency of the instrument, respectively. The spread of each type of measurement used can be described by a normal distribution. The percentage uncertainty in the sensitivity and the conversion efficiency can therefore be determined by equation SXXXIII and SXXXIV, respectively.

$$\text{Sensitvity Uncertainty} = \frac{u_{NO_{(1)}}}{NO_{(1)}} \qquad \text{(SXXXIII)}$$

$$\text{CE Uncertainty} = \sqrt{\left(\frac{u_{NO.c_{(1)}}}{NO.c_{(1)}}\right)^2 + \left(\frac{u_{NO.c_{(2)}}}{NO.c_{(2)}}\right)^2 + \left(\frac{u_{NO_{(1)}}}{NO_{(1)}}\right)^2 + \left(\frac{u_{NO_{(2)}}}{NO_{(2)}}\right)^2} \qquad \text{(SXXXIV)}$$

The drift between calibrations contains two terms; one for the sensitivity and one for the conversion efficiency when estimating the uncertainty for $NO_2$. Both terms are determined as the absolute difference between two measurements. The distribution is assumed to be rectangular as only two measurements are known – each calibration. The differences are therefore divided by $\sqrt{3}$ to get the uncertainties. To get them as percentages they are divided by last determined sensitivity and conversion efficiency, respectively. The total uncertainty in the calibration is estimated to be 2.78 ± 8.05 % for NO, 3.44 ± 9.32 % for $NO_2$ using the BLC, and 3.52 ± 8.67 % for $NO_2$ using the PLC for the calibrations between January 2014 and August 2019. The individual terms and final uncertainties in the calibrations are summarized in table S1.

Table S1: Calculated uncertainties associated with the calibrations. The values in bold are the combined uncertainties for each type of measurement. Each uncertainty is given as the mean uncertainty ± 2 standard deviation of the calibration data between January 2014 and August 2019 for NO and from March 2017 to August 2019 for both $NO_2$ measurements.

| **Source of uncertainty** | **Probability distribution** | **Uncertainty (%)** |
|---|---|---|
| Flow | Normal | 1.00 |
| Calibration gas concentration | Normal | 1.00 |
| Sensitivity | Normal | 0.16 ± 0.11 |
| Drift Sensitivity | Rectangular | 2.01 ± 8.45 |
| CE BLC | Normal | 0.44 ± 0.45 |
| Drift CE BLC | Rectangular | 1.24 ± 5.61 |
| CE PLC | Normal | 0.45 ± 0.39 |
| Drift CE PLC | Rectangular | 1.43 ± 4.86 |
| Total Calibration uncertainty NO | | **2.78 ± 8.05** |
| Total Calibration uncertainty $NO_2$ BLC | | **3.44 ± 9.32** |
| Total Calibration uncertainty $NO_2$ PLC | | **3.52 ± 8.67** |

The NO artefact is determined every night using the measurements between 21.00-03.00 UTC-1 (local time). The uncertainty can be described by a normal distribution and the uncertainty is, therefore, estimated from the standard deviation and number of the measurements used to determine the artefact. The $NO_2$ artefact is determined from measurements of PAG Zero air every 61 hours, where only 3 measurements are used for the artefact. The uncertainty is assumed to be rectangular due to the low amount of measurements used. The difference between the highest and lowest of the PAG Zero measurements is used to get the full-width. As the BLC artefact is corrected using the PLC measurement, the uncertainty in the correction is also determined in the same way and used in the propagation of uncertainties. The drift between the artefacts is estimated in the same way as the drift between the calibrations assuming a rectangular probability distribution. The total uncertainty in the NO and $NO_2$ BLC artefacts are estimated to be 1.05 ± 3.44 pptV and 7.19 ± 7.24 pptV, respectively. The individual terms and final uncertainties in the artefacts are summarized in table S2.

Table S2: Calculated uncertainties associated with the artefact determinations. The values in bold are the combined uncertainties for each type of measurement. Each uncertainty is given

as the mean uncertainty ± 2 standard deviation of the artefact data between January 2014 and August 2019 for NO and from March 2017 to August 2019 for both $NO_2$ measurements.

| **Source of uncertainty** | **Probability distribution** | **Uncertainty (pptV)** |
|---|---|---|
| NO artefact | Normal | 0.58 ± 1.07 |
| Drift NO artefact | Rectangular | 0.73 ± 3.42 |
| Total NO artefact uncertainty | | **1.05 ± 3.44** |
| $NO_2$ artefact | Rectangular | 4.58 ± 5.64 |
| $NO_2$ artefact correction | Rectangular | 0.11 ± 1.57 |
| Drift $NO_2$ artefact | Rectangular | 2.97 ± 6.73 |
| Total $NO_2$ artefact uncertainty | | **7.19 ± 7.24** |

Lastly, the uncertainty associated with correcting the measurements for $O_3$ reactions in the inlet is estimated from the uncertainties in the rate coefficient and the $O_3$ concentration. The rate coefficient used is $1.8 \times 10^{-14}$ with an uncertainty of 20% at 298K, which has been evaluated based on 6 studies of the reaction (Atkinson et al., 2004). The uncertainty in the $O_3$ concentration is ±0.07 ppbV. With measured concentrations in the range 5-60 ppbV, the uncertainty becomes 0.1-1.4%. The combined uncertainty using propagation of uncertainties, therefore, becomes 20 ± 0.001%.

The total hourly uncertainty for each of the three measurements are determined by combining all the uncertainties described using propagation of uncertainties as described in equation SXXXII. The precisions are already calculated as hourly precisions in pptV. The calibration uncertainties are interpolated between each calibration and multiplied by the hourly concentrations of NO and $NO_2$ to get hourly uncertainties in pptV. The artefact uncertainties are interpolated between each artefact determination. And the uncertainty due to ozone corrections are determined by multiplying the determined uncertainties in percentage with the hourly concentrations of NO and $NO_2$. The hourly uncertainties are determined to be 1.42 ± 1.47 pptV, 8.38 ± 7.46 pptV, and 4.44 ± 5.79 pptV for NO, $NO_2$ BLC, and $NO_2$ PLC, respectively.

# 3. FLEXPART

Back-trajectories are produced using FLEXPART, a Lagrangian particle dispersion model (Pisso et al., 2019; Stohl et al., 1998). Although originally designed to simulate dispersion of pollutants from a point source, FLEXPART has been developed into a comprehensive tool for simulating atmospheric transport. FLEXPART is run offline using meteorological reanalyses or forecasts and can be run either forwards or backwards in time, sampling particles on a global longitude-latitude-altitude grid and enabling analysis of the source regions of a plume (Stohl et al., 2003). The planetary boundary layer (PBL) height is calculated using a Richardson number threshold (Vogelezang and Holtslag, 1996), turbulence is parameterised using the standard gaussian model (Pisso et al., 2019) and the convection parameterisation is based on Emanuel and Živković-Rothman (1999). FLEXPART has been extensively evaluated and shown to be a useful and reliable resource (Forster et al., 2007; Forster et al., 2001; Stohl et al., 1998; Stohl and Trickl, 1999), particularly for investigating transport and sources of pollution (Gressent et al., 2014; Sauvage et al., 2017).

Here, FLEXPART version 10.4 is used in backwards mode, driven by pressure level data from Global Forecast System (GFS) reanalyses at 0.5°×0.5° resolution. 10-day back-trajectory simulations are initialised every 6 hours, releasing 1000 particles from the CVAO site.

# 4. Supplementary Figures:

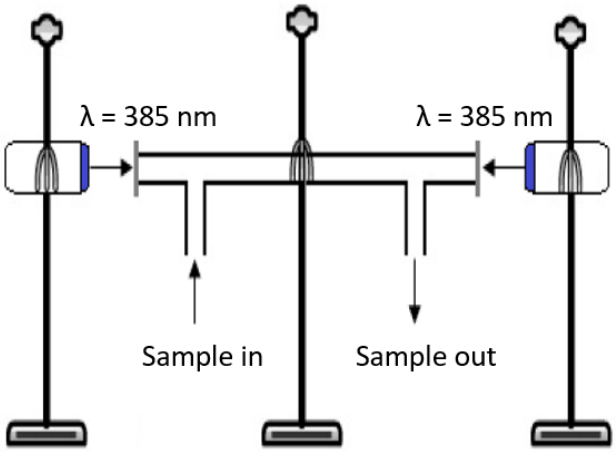


Figure S2: Diagram of the PLC (not to scale). The quartz tube is held in place by a clamp and clamp stand. Two Hamamatsu Lightningcure V3 diodes (λ = 385 nm) are positioned with the light source facing towards the tube, leaving approximately 2 mm distance between the diode and the glass window of the tube. Diodes are held in place with a clamp and clamp stand.

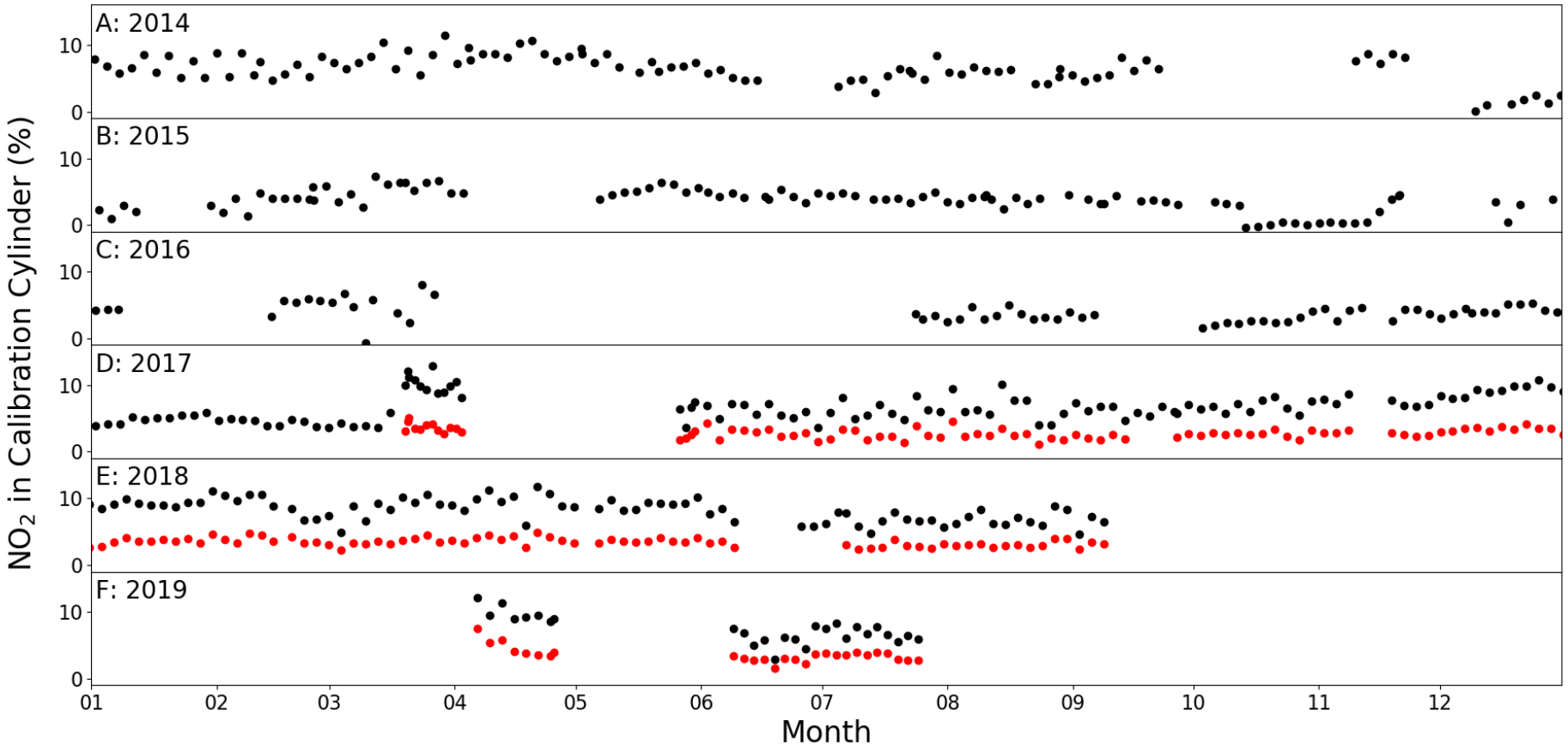


Figure S3: Percentage of $NO_x$ in the calibration cylinder measured as $NO_2$ between January 2014 and August 2019. The black circles symbolise the measurements made by the BLC and the red circles symbolise the measurements made by the PLC.

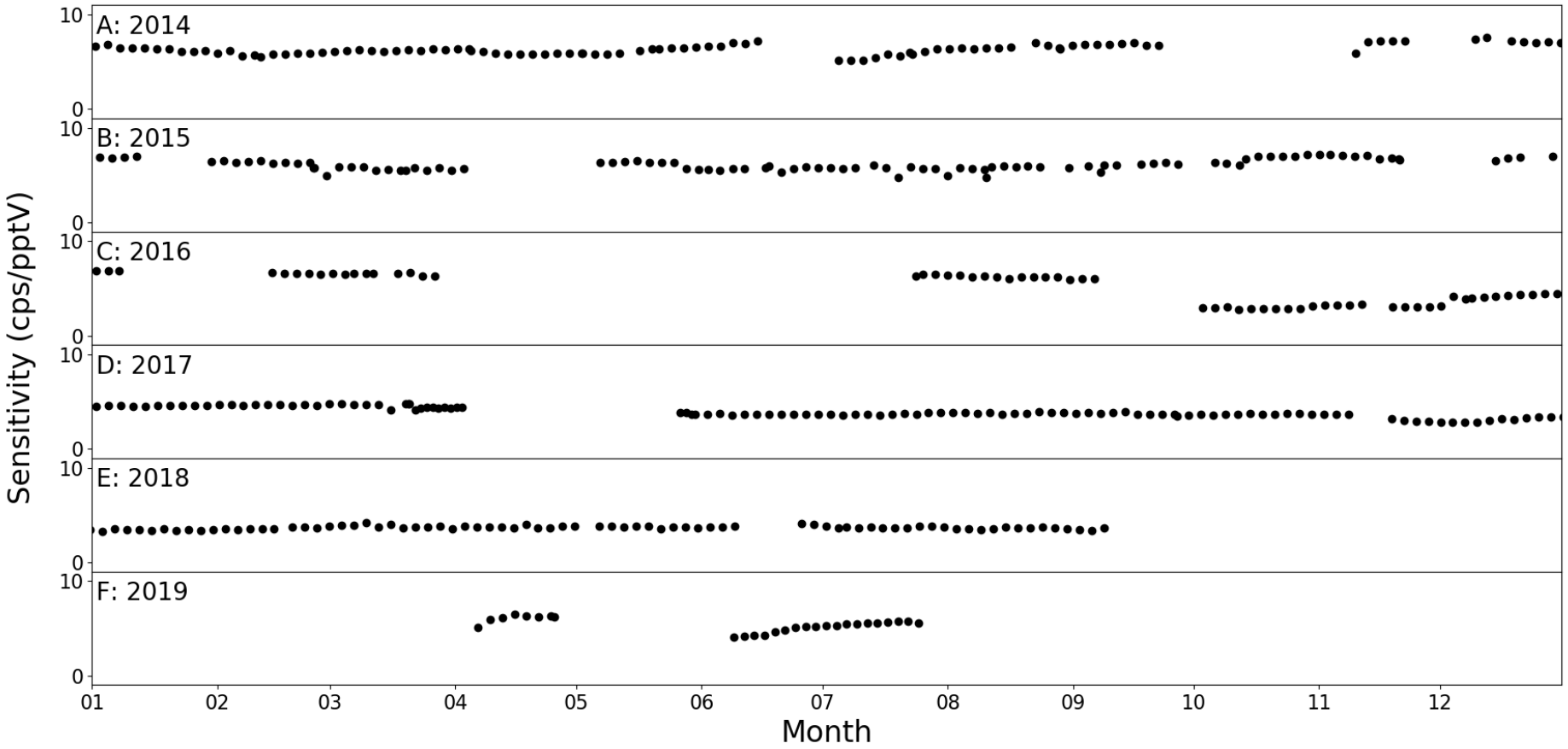


Figure S4: Calculated sensitivities between January 2014 and August 2019.

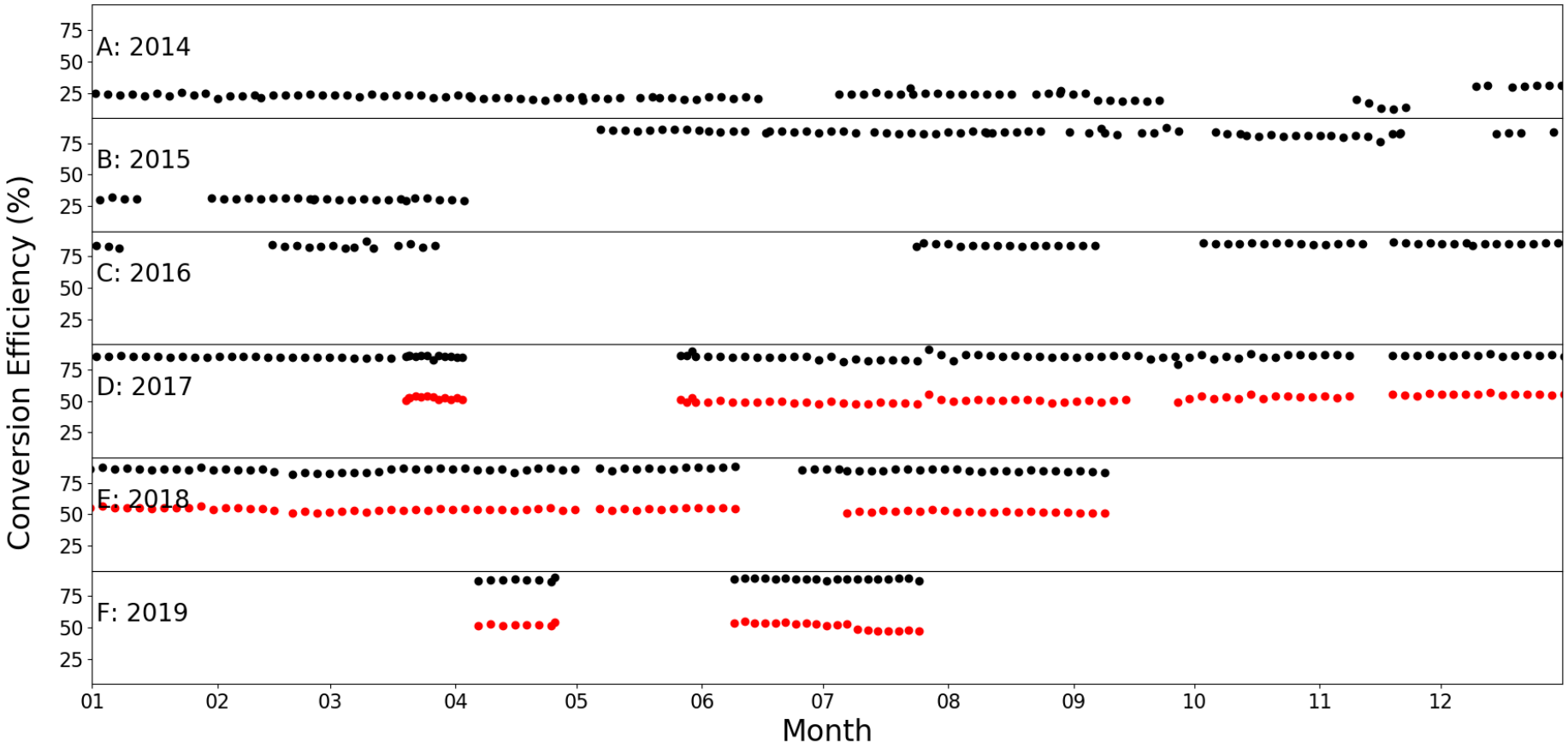


Figure S5: Calculated conversion efficiencies for the BLC (black) and PLC (red) from January 2014 to August 2019.

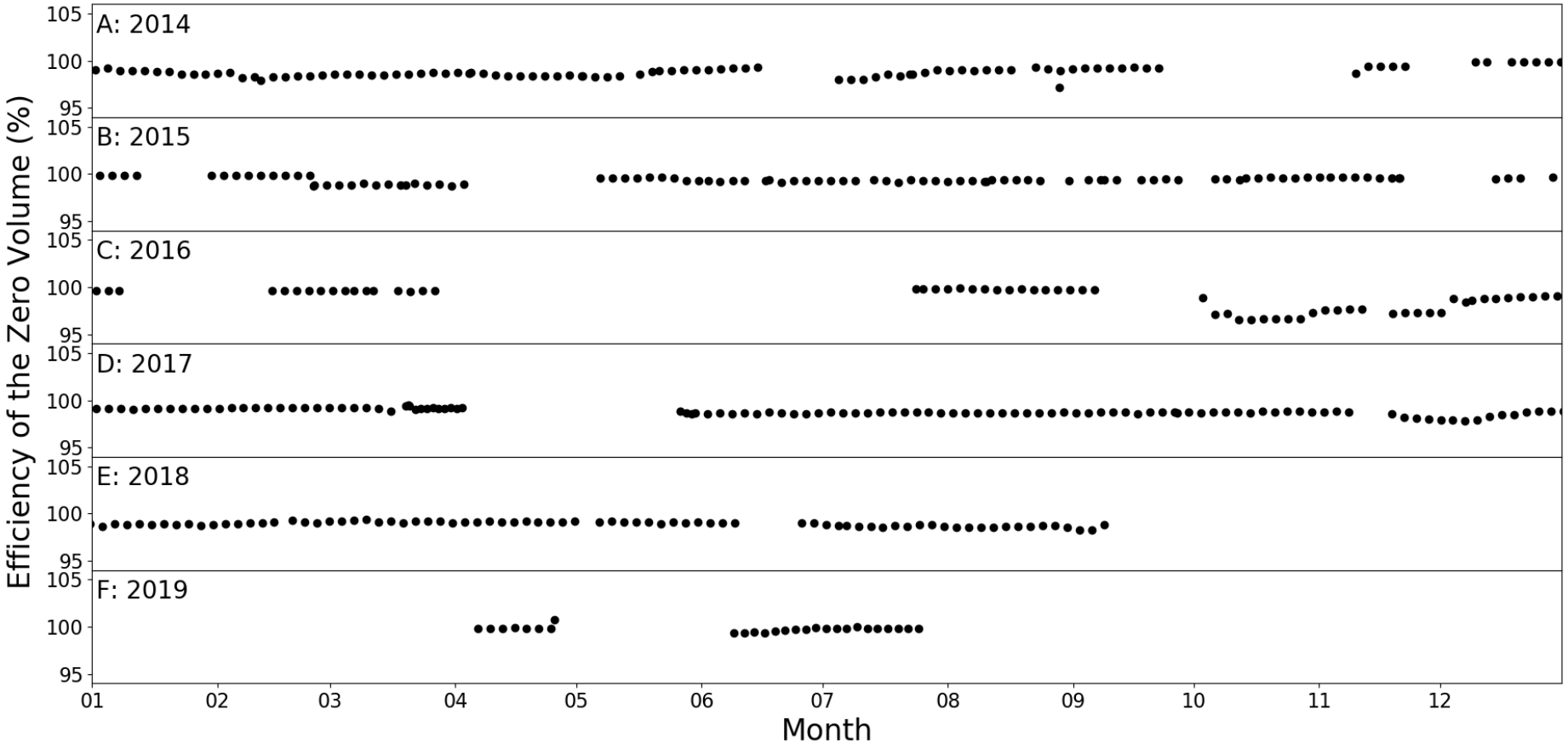


Figure S6: The efficiency of the zero volume plotted over time from January 2014 to August 2019.

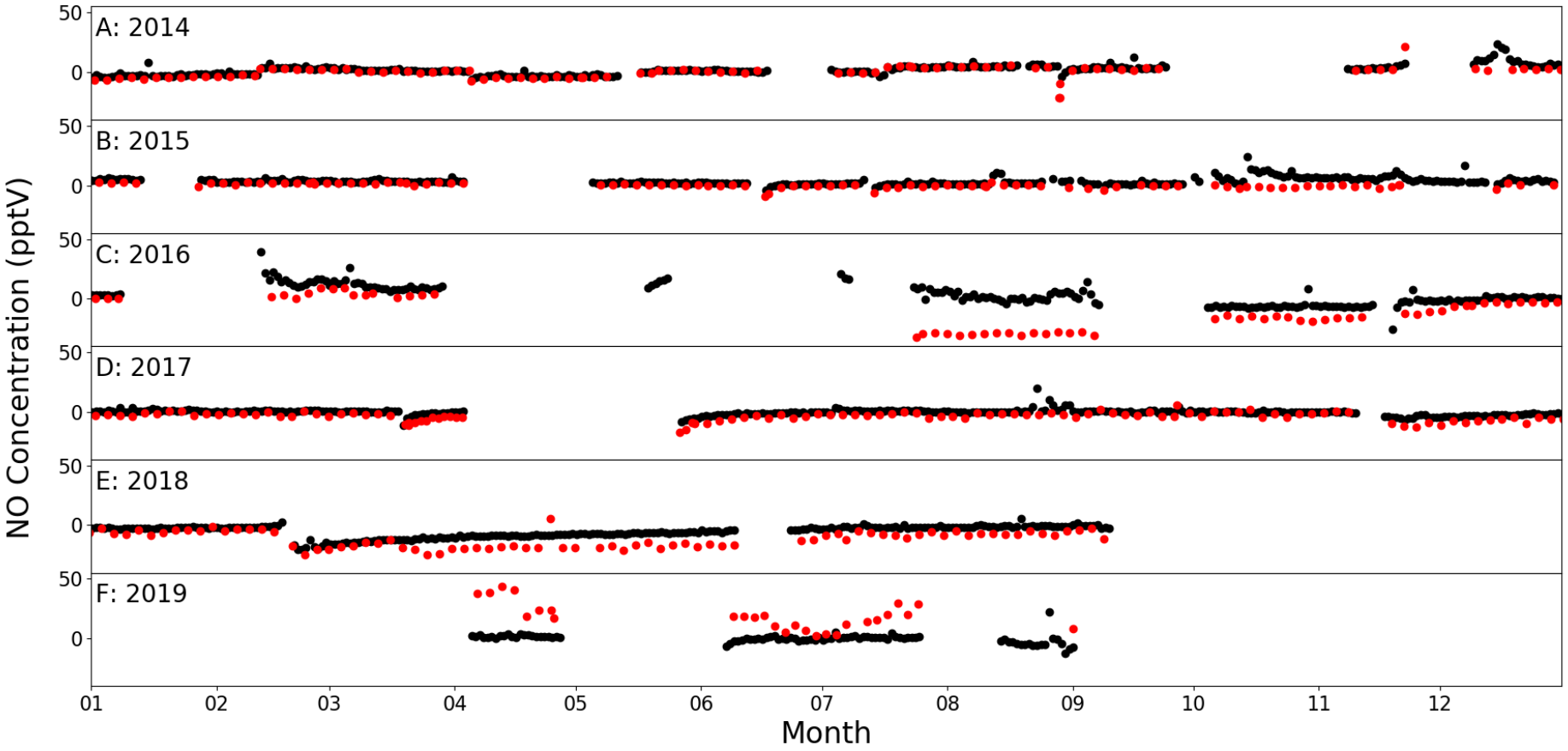


Figure S7: NO artefact from January 2014 to August 2019, where the black is the average night time measurements and the red are the measurements from the pure air generator (PAG).

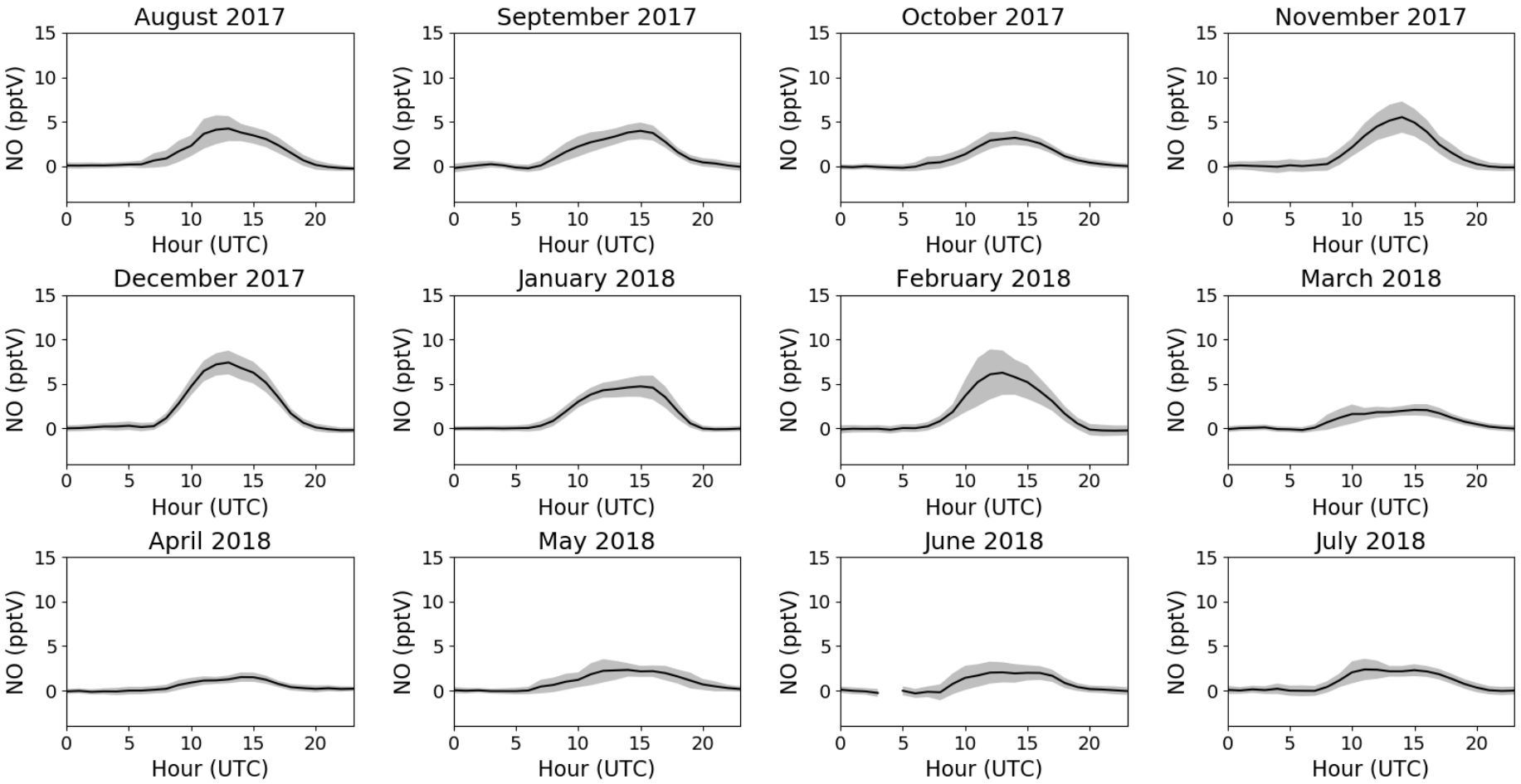


Figure S8: NO diurnals for August 2017-July 2018. The coloured area is ±2 standard errors. If there are less than 15 measurements available for the hour, it is not included.

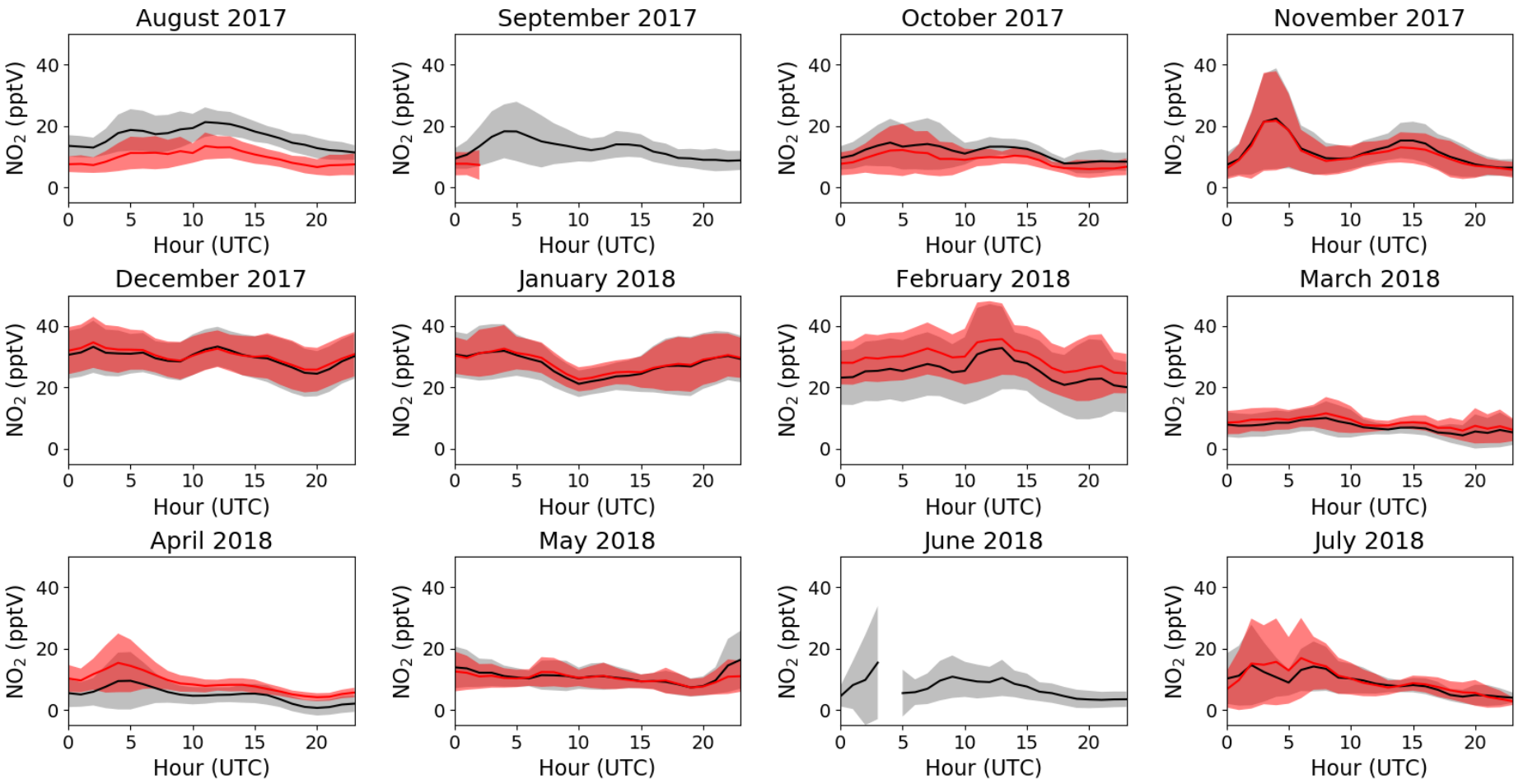


Figure S9: $NO_2$ diurnals for August 2017-July 2018 for the BLC (black) and PLC (red). The coloured area is ±2 standard errors. If there are less than 15 measurements available for the hour, it is not included.

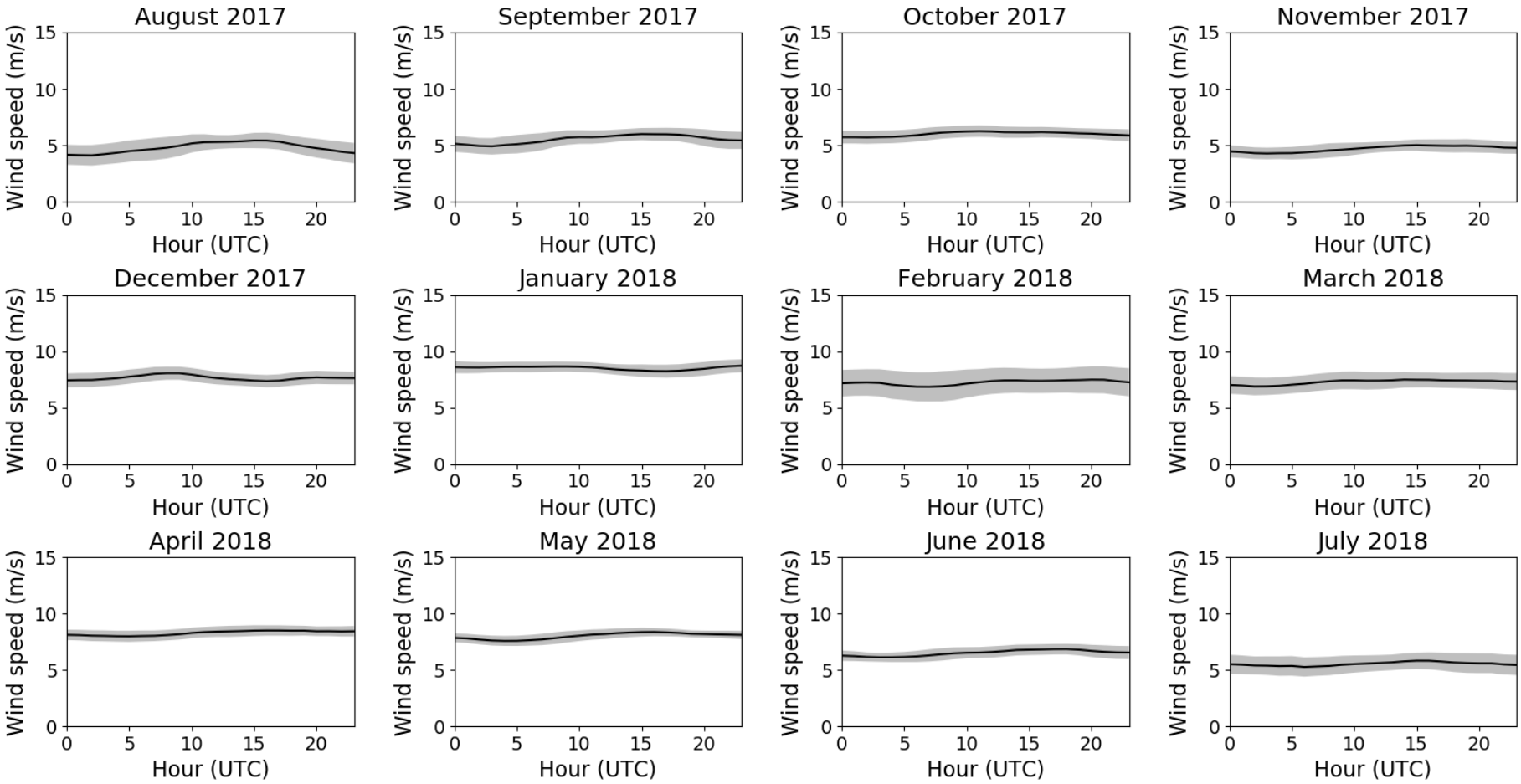


Figure S10: Wind speed diurnals for August 2017-July 2018. The coloured area is ±2 standard errors. If there are less than 15 measurements available for the hour, it is not included.

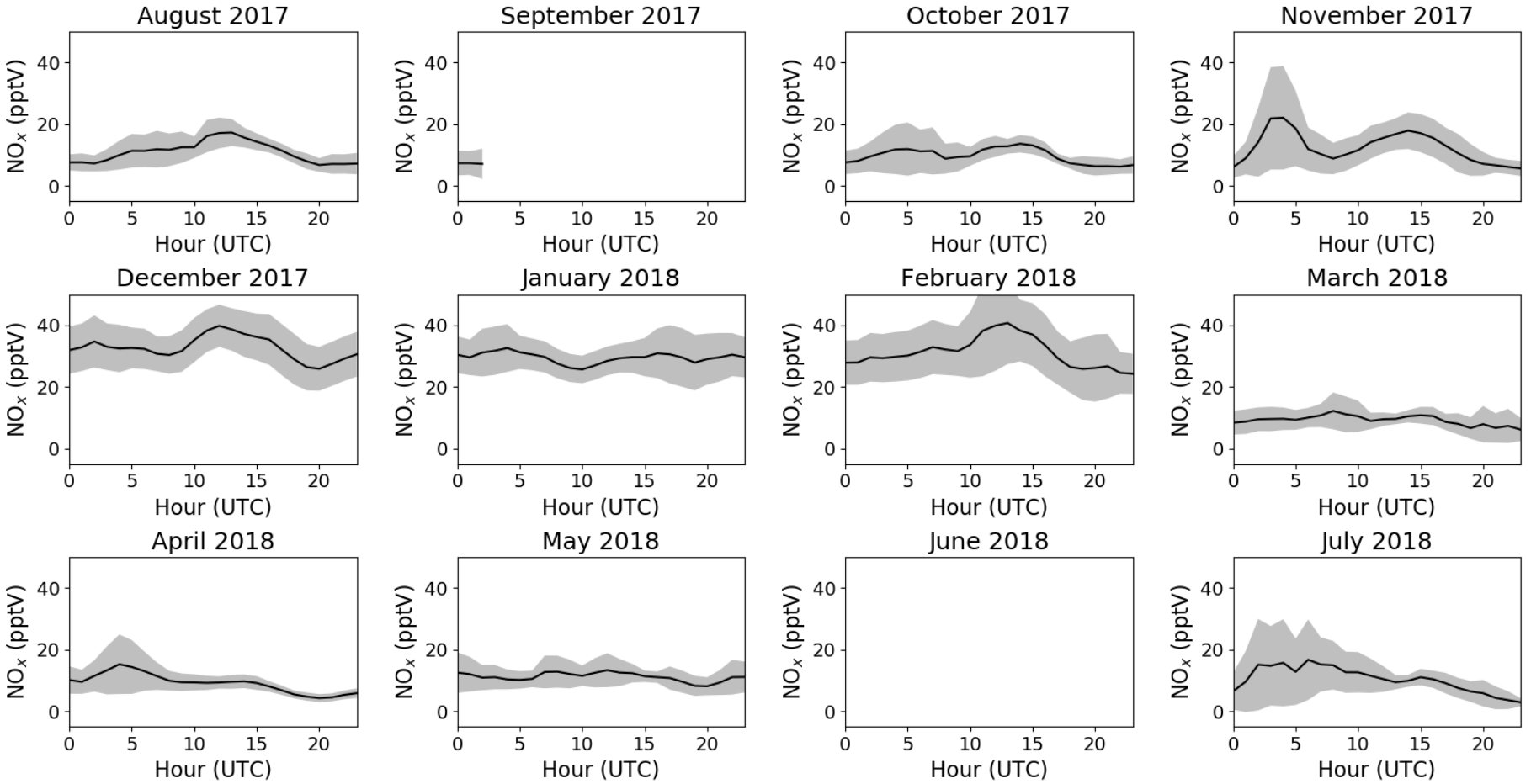


Figure S11: $NO_x$ diurnals for August 2017-July 2018. The coloured area is ±2 standard errors. If there are less than 15 measurements available for the hour, it is not included.

# 5. References


Atkinson, R., Baulch, D. L., Cox, R. A., Crowley, J. N., Hampson, R. F., Hynes, R. G., Jenkin, M. E., Rossi, M. J., and Troe, J.: Evaluated kinetic and photochemical data for atmospheric chemistry: Volume I - gas phase reactions of Ox, HOx, NOx and SOx species, Atmos. Chem. Phys., 4, 1461-1738, 10.5194/acp-4-1461-2004, 2004.

Bell, S.: A Beginner's Guide to Uncertainty of Measurement, NPL, 1999.

Emanuel, K. A., and Živković-Rothman, M.: Development and Evaluation of a Convection Scheme for Use in Climate Models, Journal of the Atmospheric Sciences, 56, 1766-1782, 10.1175/1520-0469(1999)056<1766:Daeoac>2.0.Co;2, 1999.

Forster, C., Wandinger, U., Wotawa, G., James, P., Mattis, I., Althausen, D., Simmonds, P., O'Doherty, S., Jennings, S. G., Kleefeld, C., Schneider, J., Trickl, T., Kreipl, S., Jäger, H., and Stohl, A.: Transport of boreal forest fire emissions from Canada to Europe, Journal of Geophysical Research: Atmospheres, 106, 22887-22906, 10.1029/2001jd900115, 2001.

Forster, C., Stohl, A., and Seibert, P.: Parameterization of Convective Transport in a Lagrangian Particle Dispersion Model and Its Evaluation, Journal of Applied Meteorology and Climatology, 46, 403-422, 10.1175/jam2470.1, 2007.

Gressent, A., Sauvage, B., Defer, E., Pätz, H. W., Thomas, K., Holle, R., Cammas, J.-P., Nédélec, P., Boulanger, D., Thouret, V., and Volz-Thomas, A.: Lightning NOx influence on large-scale NOy and O3 plumes observed over the northern mid-latitudes, Tellus B: Chemical and Physical Meteorology, 66, 25544, 10.3402/tellusb.v66.25544, 2014.

Lee, J. D., Moller, S. J., Read, K. A., Lewis, A. C., Mendes, L., and Carpenter, L. J.: Year-round measurements of nitrogen oxides and ozone in the tropical North Atlantic marine boundary layer, J Journal of Geophysical Research: Atmospheres, 114, 2009.

Pisso, I., Sollum, E., Grythe, H., Kristiansen, N. I., Cassiani, M., Eckhardt, S., Arnold, D., Morton, D., Thompson, R. L., Groot Zwaaftink, C. D., Evangeliou, N., Sodemann, H., Haimberger, L., Henne, S., Brunner, D., Burkhart, J. F., Fouilloux, A., Brioude, J., Philipp, A., Seibert, P., and Stohl, A.: The Lagrangian particle dispersion model FLEXPART version 10.4, Geosci. Model Dev., 12, 4955-4997, 10.5194/gmd-12-4955-2019, 2019.

Reed, C., Evans, M. J., Crilley, L. R., Bloss, W. J., Sherwen, T., Read, K. A., Lee, J. D., and Carpenter, L. J.: Evidence for renoxification in the tropical marine boundary layer, Atmos. Chem. Phys., 17, 4081-4092, 10.5194/acp-17-4081-2017, 2017.

Sauvage, B., Fontaine, A., Eckhardt, S., Auby, A., Boulanger, D., Petetin, H., Paugam, R., Athier, G., Cousin, J. M., Darras, S., Nédélec, P., Stohl, A., Turquety, S., Cammas, J.-P., and Thouret, V.: Source attribution using FLEXPART and carbon monoxide emission inventories: SOFT-IO version 1.0, Atmospheric Chemistry and Physics Discussions, 1-48, 10.5194/acp-2017-653, 2017.

Silvia, D., and Skilling, J.: Data Analysis: A Bayesian Tutorial, 2nd ed., Oxford Univ. Press, Oxford, U. K., 2006.

Stohl, A., Hittenberger, M., and Wotawa, G.: Validation of the lagrangian particle dispersion model FLEXPART against large-scale tracer experiment data, Atmospheric Environment, 32, 4245-4264, https://doi.org/10.1016/S1352-2310(98)00184-8, 1998.

Stohl, A., and Trickl, T.: A textbook example of long-range transport: Simultaneous observation of ozone maxima of stratospheric and North American origin in the free troposphere over Europe, Journal of Geophysical Research: Atmospheres, 104, 30445-30462, 10.1029/1999jd900803, 1999.

Stohl, A., Forster, C., Eckhardt, S., Spichtinger, N., Huntrieser, H., Heland, J., Schlager, H., Wilhelm, S., Arnold, F., and Cooper, O.: A backward modeling study of intercontinental pollution transport using aircraft measurements, Journal of Geophysical Research: Atmospheres, 108, 10.1029/2002jd002862, 2003.

Vogelezang, D. H. P., and Holtslag, A. A. M.: Evaluation and model impacts of alternative boundary-layer height formulations, Boundary-Layer Meteorology, 81, 245-269, 10.1007/BF02430331, 1996.